Lawrence Berkeley National Laboratory
LBL Publications

Title
The first back-side illuminated types of Kyoto's X-ray astronomy SOIPIX

Permalink
https://escholarship.org/uc/item/6t9658k2

Authors
Itou, Makoto
Tsuru, Takeshi Go
Tanaka, Takaaki
et al.

Publication Date
2016-09-01

DOI
10.1016/j.nima.2016.04.012

Peer reviewed

eScholarship.org Powered by the California Digital Library
University of California

Nuclear Instruments and Methods in Physics Research A 831 (2016) 55–60

Contents lists available at ScienceDirect

Nuclear Instruments and Methods in Physics Research A

journal homepage: www.elsevier.com/locate/nima

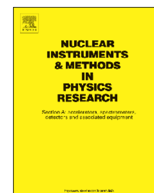

The first back-side illuminated types of Kyoto's X-ray astronomy SOIPIX

Makoto Itou [a,*], Takeshi Go Tsuru [a], Takaaki Tanaka [a], Ayaki Takeda [a], Hideaki Matsumura [a], Shunichi Ohmura [a], Hiroyuki Uchida [a], Shinya Nakashima [b], Yasuo Arai [c], Ikuo Kurachi [c], Koji Mori [d], Ryota Takenaka [d], Yusuke Nishioka [d], Takayoshi Kohmura [e], Koki Tamasawa [e], Craig Tindall [f]

[a] Department of Physics, Graduate School of Science, Kyoto University, Kitashirakawa Oiwake-cho, Sakyo-ku, Kyoto 606-8502, Japan
[b] Institute of Space and Astronautical Science (ISAS)/JAXA, 3-1-1 Yoshinodai, Chuo-ku, Sagamihara, Kanagawa 252-5210, Japan
[c] Institute of Particle and Nuclear Studies, High Energy Accelerator Research Org., KEK, 1-1 Oho, Tsukuba 305-0801, Japan
[d] Department of Applied Physics, Faculty of Engineering, University of Miyazaki,1-1 Gakuen Kibana-dai Nishi, Miyazaki 889-2192, Japan
[e] Department of Physics, Faculty of Science and Technology, Tokyo University of Science, 2641 Yamazaki, Noda, Chiba 278-8510, Japan
[f] Lawrence Berkeley National Laboratory, Berkeley, CA 94720, USA

ARTICLE INFO

Article history:
Received 10 January 2016
Received in revised form
1 April 2016
Accepted 6 April 2016
Available online 7 April 2016

Keywords:
X-ray SOIPIX
Monolithic silicon pixel detector
Silicon on insulator technology

ABSTRACT

We have been developing Kyoto's X-ray astronomy SOI pixel sensors, called "XRPIX", aiming to extend the frontiers of X-ray astronomy with the wide-band imaging spectroscopy in the 0.5–40 keV band. A dead layer on the X-ray incident surface should ideally be as thin as possible to achieve a high sensitivity below 1 keV, and the depletion layer is required to be thick enough to detect 40 keV X-rays. Thus, we have started developing fully-depleted back-side illuminated (BI) types of XRPIXs. This paper reports on our first two BI devices and their X-ray evaluation (2.6–12 keV). The device named "XRPIX2b-FZ-LA" successfully reaches a full depletion with a thickness of 500 μm. On the other hand, it has a dead layer with a thickness of 1.1–1.5 μm and struggles to achieve the requirement of 1.0 μm. The other device named "XRPIX2b-CZ-PZ", which is applied with a thin Si sensor-layer and an improved back-side process, is found to satisfy the requirement with its thickness of 0.9–1.0 μm, including Al optical blocking filter of 0.2 μm, although the Si sensor-layer is rather thin with 62 μm. We also describe in this paper the X-ray calibration system that we have built for the X-ray evaluation of XRPIXs.

© 2016 Elsevier B.V. All rights reserved.

1. Introduction

Charge-coupled devices (CCDs) have opened a new era of X-ray astronomy with their superior abilities of fine imaging and Fano-limited spectroscopy (e.g. [1–4]). However, the upper bound of the observable energy is ~ 10 keV due to high non-X-ray background (NXB) induced by the interaction with cosmic-rays in orbit [5]. In order to reduce NXB, we adopt an anti-coincident technique with scintillators surrounding an X-ray imager. Since the counting rate of the scintillators is estimated to be around ~kHz in a low earth orbit [6,7], the X-ray imager is required to have higher time resolution than ~msec by at least one order of magnitude. The latest versions of X-ray CCDs and active pixel sensors currently under development can hardly satisfy the requirement [8–13]. So, we have been developing a new type of active pixel sensors with a high time resolution, "XRPIXs", for the next-generation wide-band X-ray imaging spectroscopy in the energy range of 0.5–40 keV [14].

We equip the XRPIX with a function to output trigger signals and the corresponding hit-pixel addresses, with which it achieves a high time-resolution of better than ~ 10 μs. It also allows us to adopt an anti-coincident technique and observe faint sources above ~10 keV at low non-X-ray background.

The XRPIXs are monolithic active sensors processed with silicon-on-insulator (SOI) CMOS technology [15]. The device consists of three layers of a low-resistivity Si-bonded wafer for high-speed CMOS circuits (~8 μm in thickness), a thick high-resistivity depleted Si-layer for X-ray detection, and SiO_2 insulator between the two (Fig. 1).

The depletion layer spreads from p+ in the Si sensor-layer toward the back side. The depletion layer is required to be thick enough to detect X-rays with the energies above ~ 10 keV, and our goal is 500 μm in thickness. Since the front-side of the XRPIX has a circuitry layer of 8 μm thick, which undesirably blocks much of low-energy X-rays below ~1 keV, we adopt back-side illumination (BI) in order to obtain high sensitivity for low-energy X-rays. Thus, the fully depleted BI-type of the XRPIXs is essential to achieve the wide-bandpass performance. At present we are aiming at 1.0 μm in thickness for the dead-layer, whereas our goal is 0.1 μm. In this

* Corresponding author.
E-mail address: itou@cr.scphys.kyoto-u.ac (M. Itou).

http://dx.doi.org/10.1016/j.nima.2016.04.012
0168-9002/© 2016 Elsevier B.V. All rights reserved.

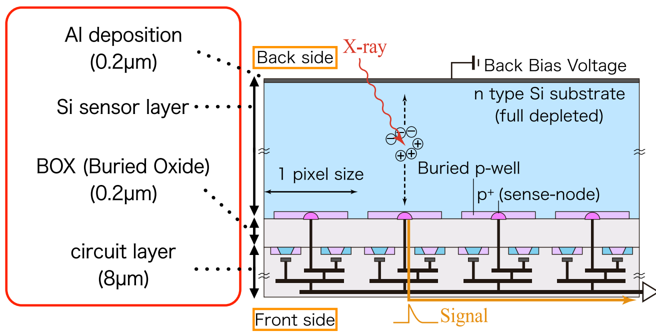

Fig. 1. The cross-sectional view of SOIPIX.

paper, we first describe the X-ray calibration system that we have developed, and then report the X-ray performance of the first devices of the BI-types of XRPIXs, "XRPIX2b-FZ-LA" and "XRPIX2b-CZ-PZ".

2. X-ray calibration system

We have developed an X-ray calibration system of XRPIXs, using fluorescent X-ray lines at various energies. This system was originally the calibration system used for the X-ray Imaging Spectrometer (XIS) of the Suzaku satellite [16], and some modifications have been made. The system consists of two vacuum chambers as illustrated in Fig. 2. Vacuum chamber 1 is equipped with an X-ray tube (Oxford 5000 series) for primary X-ray generation and eight secondary targets placed on a rotating stage. We can easily change the secondary X-ray target by rotating the stage. An XRPIX and its readout printed circuit boards are installed in vacuum chamber 2. A pulse tube cooler (Iwatani CryoMini P003) is equipped with the chamber to cool the XRPIX to −50 °C. We use a readout system consisting of a sub-board on which the XRPIX is attached, and a SEABAS (Soi EvAluation BoArd with Sitcp) board. Details of the SEABAS board are reported in [17].

We used four secondary targets of Cl, Ti, Fe and Se out of the eight in this paper. Before the performance evaluation of XRPIXs, we observed the spectra of the Cl-K, Ti-K, Fe-K, and Se-K lines with a silicon drift detector (SDD: Amptek XR-100). We obtained the absolute fluxes of the lines at the position of the XRPIX, referring to the quantum efficiency and collimator size of the SDD given in the Amptek website [18], and correcting the difference in the distances from the secondary target to the XRPIX and SDD. Table 1 summarizes the results. The errors are dominated by the systematic error of the collimator area of the SDD (±10%). All errors

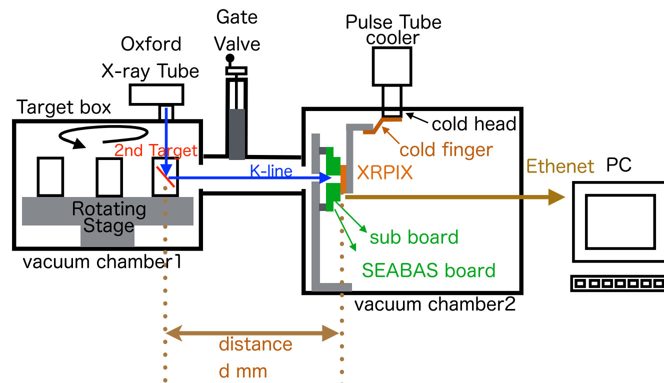

Fig. 2. The schematic view of the X-ray calibration system for XRPIX. The distance *d* from the secondary target to the XRPIX is 509 mm whereas the one to the SDD is 475 mm.

Table 1
X-ray flux at the position of the XRPIX.

Fluorescent X-ray line	Energy (keV)		Flux (ph/mm^2/s)[a]
	Kα	Kβ	
Cl-K	2.6	2.8	3.3 ± 0.3
Ti-K	4.5	4.9	0.52 ± 0.05
Fe-K	6.4	7.1	0.46 ± 0.04
Se-K	11.2	12.5	0.70 ± 0.07

[a] The sum of the Kα and Kβ lines.

in this paper represent 90% confidence range for one parameter unless otherwise noted.

3. XRPIX2b-FZ-LA

3.1. Device description

We began the development of the BI types of XRPIXs with the device "XRPIX2b-FZ-LA", whose specifications are summarized in Table 2. The XRPIX2bs are the fourth devices in the XRPIX series [19] and are fabricated by LAPIS Semiconductor Co. Ltd., using a 0.2 μm fully depleted SOI CMOS Pixel process. This device is suitable for testing of back-side illumination because it has been well studied [19–21] and includes a large detector (6.0 mm × 6.0 mm consisting of 152 × 152 pixels) compared with the other XRPIXs.

We have used two types of Si sensor-layers for XRPIXs in terms of resistivity. One is the Floating Zone (FZ) device with the nominal resistivity of ~4 kΩ cm, and the other is the Czochralski (CZ) with ~1.2 kΩ cm. The XRPIX2b-FZ-LAs have the FZ-type sensor-layer with the thickness of 500 μm. The ion implantation was performed on the back-side of the device after the chemical etching in order for the back-side to have electrical contact with the back-bias voltage. This process was followed by laser annealing and vapor-deposition of an Al layer with 0.2 μm thickness for optical blocking.

Fig. 3 shows the results with the secondary ion mass spectrometry (SIMS) and spreading resistance analysis (SRA) on a device which is made with the same back-side process as the one measured with X-rays. It indicates that the phosphorus layer extends to a depth of ~ 0.5 μm from the back-side surface. We note that the Al optical-blocking layer of 0.2 μm is not included in these analyses.

3.2. Experiments and results

With the XRPIX2b-FZ-LA, we obtained spectra and count rates of the K-line X-rays of Cl, Ti, Fe and Se with several back-bias voltages (V_{bb}) from 160 V to 300 V, using the calibration system described in Section 2. The device was cooled to −50 °C at a degree of vacuum lower than 10^{-5} Torr. We performed a frame-by-

Table 2
Specifications of XRPIX2b-FZ-LA and -CZ-PZ.

Specification	XRPIX2b-FZ-LA	XRPIX2b-CZ-PZ
Pixel size (μm × μm)	30 × 30	
Format (pixels)	152 × 152	
Wafer type	Floating zone	Czochralski
Nominal resistivity (k Ω cm)	~4	~1.2
Sensor layer (μm)	500	62
Back-side process	Ion implantation, Laser annealing	Pizza process
Al deposition	0.2 μm	None

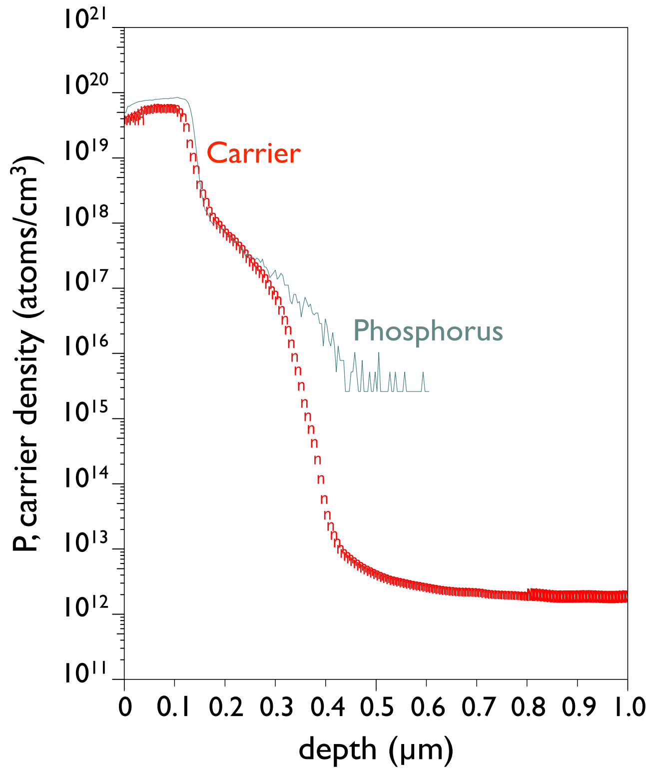

Fig. 3. Phosphor concentration profile on the back-side, obtained with SIMS and SRA of XRPIX2b-FZ-LA. Note that the thickness of the Al optical-blocking layer is not included in the depth in the profile.

frame readout, where all the pixels are sequentially read after a 10 ms exposure. The detail of this readout sequence is reported in [22]. We analyzed the data according to the methods given in [22,23]. After extracting X-ray event data, of which the pixel output exceeds the event threshold, we classified each X-ray event into four grades of "single pixel", "double pixels", "triple pixels" or "other" according to the split threshold. The readout noise was 61e$^-$ (0.2 keV). The event threshold and the split threshold were set to be 6σ (1.3 keV) and 3σ (0.6 keV) of the readout noise, respectively. We note that Takeda et al. (2015) discuss the nature and source of the readout noise extensively [20].

Fig. 4shows the quantum efficiencies as a function of X-ray energy, where the QE is defined as the ratio of a counting rate

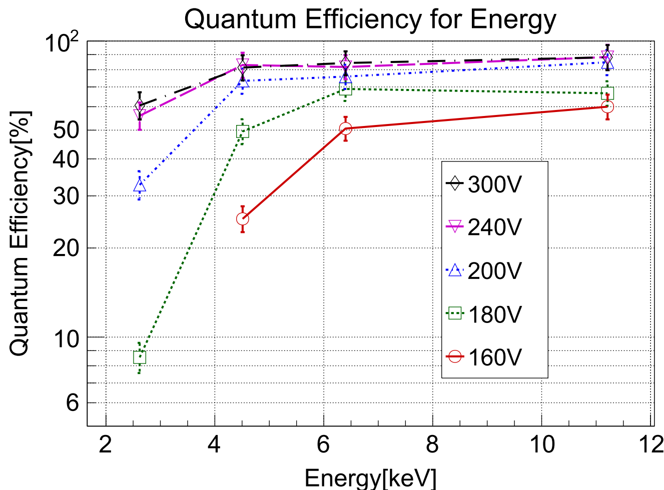

Fig. 4. Quantum efficiency of XRPIX2b-FZ-LA as a function of X-ray energy for various back-bias voltages.

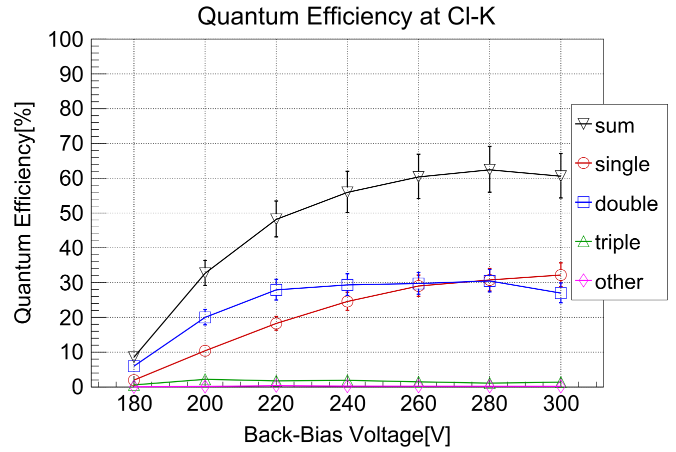

Fig. 5. Quantum efficiency of each grade with XRPIX2b-FZ-LA at the energy of Cl-K X-rays as a function of V_{bb}.

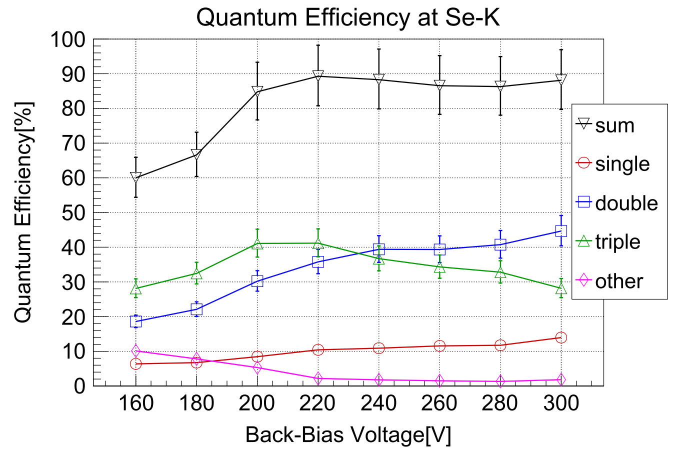

Fig. 6. Same as Fig. 5 but at the energy of Se-K X-rays.

detected by the XRPIX to the illuminated absolute flux. The QEs shown in Fig. 4 are those with the sum of the four grades. Figs. 5 and 6 show the QE of each grade separately as a function of the applied back-bias voltages. The QE with the sum of the four grades increases as a higher back-bias voltage is applied, but is saturated at $V_{bb} \geq 260$ V. The observed QE for the Se-K line is consistent with the expected value for absorption by Si sensor-layer of 500 μm thick. This result suggests that the Si sensor-layer gets fully depleted at ~260 V.

From the QE at the energy of Cl-K X-rays alone, the thickness of the dead layer on the back-side is estimated to be 1.5 ± 0.3 μm, including the Al optical blocking layer of 0.2 μm thick. The error in the estimate comes mainly from the uncertainty in the SDD collimator area. We obtain the thickness of 1.1 ± 0.2 μm from the ratio between the counting rates of Cl-K and Ti-K lines, of which the estimate is independent of the uncertainty in the SDD collimator area. The two estimations are consistent with each other.

3.3. QE at a low X-ray energy

The experiments with "XRPIX2b-FZ-LA" show that we can basically reach a full depletion layer of 500 μm thick in the sensor layer at $V_{bb} \geq 260$ V. On the other hand, it does not achieve the requirement of 1.0 μm for the thickness of the dead layer. In this section, we discuss methods to improve the QE at a low X-ray energy in the region where the full depletion is achieved by applying a high back-bias voltage.

The charge generated by an X-ray photon absorbed near the

back-side is shared by multiple pixels due to the lateral diffusion while the charge is drifting toward the front-side in the thick depletion layer. An event produced by a Se-K X-ray with the energy of 11–12 keV has at least one pixel with charge larger than the event threshold of 1.3 keV even if its signal charge splits into four pixels. The charge generated by an Se-K X-ray is also much higher than the split threshold of 0.6 keV. Thus, almost all the events are expected to be detected as X-ray events, and many of the events are regarded as not single-pixel events but multiple-pixel events.

On the other hand, the Cl-K energy of 2.6 keV is only twice of the event threshold of 1.3 keV. Therefore, when a photon of 2.6 keV creates a charge cloud in the sensor layer, if the generated cloud spreads on more than 2 pixels and if a part of the cloud in none of the pixels has the energy exceeding 1.3 keV, it is not regarded as an X-ray event. As a result, many events involving three or more pixels are expected to be missed. We also expect that the fraction of single-pixel events to the total events for Cl-K X-rays is higher than that for Se-K X-rays, since the split threshold of 0.6 keV is as high as ~1/4 of the Cl-K energy of 2.6 keV. Thus, the first method that we are planning to adopt is to recover the missing three- or more pixel events by adopting a low event threshold. Adopting a low event threshold requires a low readout noise. This method will be done with the devices with a lower readout noise such as XRPIX3b [20].

It is also effective to increase the branching ratio of single-pixel events by applying as high back-bias voltage as possible, where the branching ratio is defined as the fraction of the events with each grade in the total number of events. The branching ratio changes according to the back-bias voltage even in the region of $V_{bb} \geq 260$ V (Figs. 5 and 6). The branching ratios of single-pixel and double-pixel events of Se-K X-rays increase as the back-bias voltage is increased, whereas that of the triple-pixel events decreases. Similar tendency is observed in the branching ratios of single-pixel and double-pixel events of Cl-K X-rays. The cause of this tendency is interpreted as follows. After the full depletion is reached, the intensity of electric field in the Si sensor-layer increases as a higher back-bias voltage is applied. The strong electric field prevents a signal charge-cloud from expanding in the Si sensor-layer. This suggests that it would be possible to further increase less expanded events by applying back-bias voltage higher than 300 V, which is the second method. We have to note that a high back-bias voltage would damage the device due to an electric discharge. Unfortunately, we have had only a small number of experiences in applying a back-bias voltage higher than 300 V to the XRPIX2b devices. Since we cannot damage precious BI devices, this method is a subject of future investigation.

The third method is that we increase the branching ratio of the single-pixel events by thinning the Si sensor-layer and preventing the charge cloud from diffusing widely. We note that some optimization is necessary to thin it, because a thin Si sensor-layer reduces the QE at a high X-ray energy.

The device has a dead layer with a thickness of ~1 μm. The attenuation lengths for 2.5 keV and 0.5 keV X-rays are 3.0 μm and 0.43 μm, respectively. Reduction of the thickness of the dead layer itself increases the QE in the low X-ray energy band. Thus, the fourth method is that we adopt another back-side process to thin the dead layer itself.

In the following section, we report the results of a device, to which the third and fourth methods are applied.

4. XRPIX2b-CZ-PZ

4.1. Device description

We fabricated the device, "XRPIX2b-CZ-PZ", which has a thin Si sensor-layer of 62 μm thickness (the third method in Section 3) and the back-side treated with the "Pizza process" (the fourth method), developed by LBNL [24]. The specifications of the device are given in Table 2. The Pizza process goes through the following procedure. Following the thinning of the device, a thin phosphorus layer is implanted at 33 keV in a cold environment at a temperature of −160 °C, and finally the device is annealed at ~ 500 °C for ~10 min. An amorphous layer is formed at the back-side to have electrical contact. After a XRPIX2b-CZ device with a thickness of 260 μm had been produced by LAPIS Semiconductor Co. Ltd. in Japan, it was post-processed with back-thinning and formation of an amorphous layer in LBNL. The thickness of the phosphor layer was found to be ~0.4 μm with the SIMS (Fig. 7) and SRA (Fig. 1 in [24]).

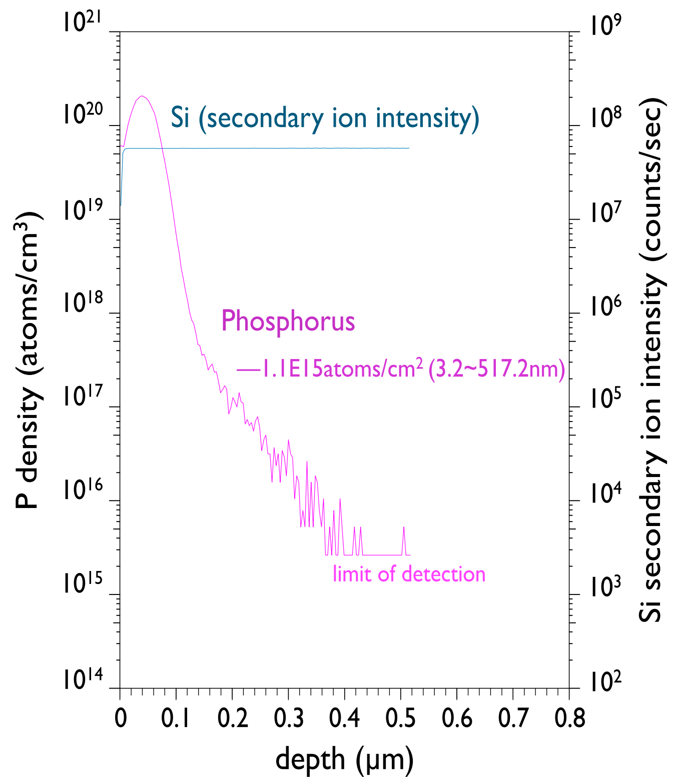

Fig. 7. Phosphor concentration profile on the back-side from SIMS of XRPIX2b-CZ-PZ.

4.2. Experiments and results

We obtained the X-ray performance of XRPIX2b-CZ-PZ with the same setting of experiments as those done for the XRPIX2b-FZ-LA but with V_{bb} of 20–70 V. The readout noise was 61 e^- (0.2 keV), which is the same as that of XRPIX2b-FZ-LA. We used the same event and split thresholds as those used for XRPIX2b-FZ-LA in the analyses. Fig. 8 shows the QEs as a function of X-ray energy, and Figs. 9 and 10 show the QEs as a function of back-bias voltages at the X-ray energies of Cl-K and Se-K lines, respectively. We found that the full depletion was achieved at V_{bb} of 60 V. The QE at the X-ray energy of the Se-K lines is consistent with that predicted with the thickness of the Si sensor-layer. The branching ratio of the single pixel of the Cl-K X-ray events is significantly higher than that with XRPIX2b-FZ-LA, as expected.

We found the thickness of the dead layer to be 0.8 ± 0.3 μm from the QE at the energy of Cl-K lines and 0.7 ± 0.2 μm from the ratio between the count rates of Cl-K and Ti-K lines, both of which are consistent with each other.

By including an Al optical blocking layer of 0.2 μm, the dead

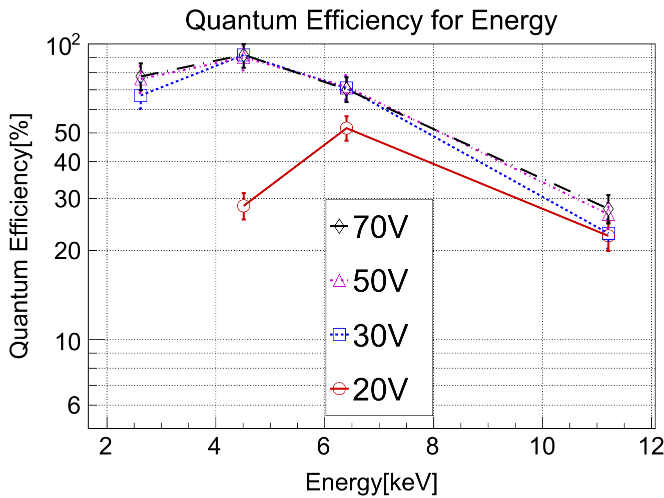

Fig. 8. Quantum efficiency of XRPIX2b-CZ-PZ as a function of X-ray energy for various back-bias voltages.

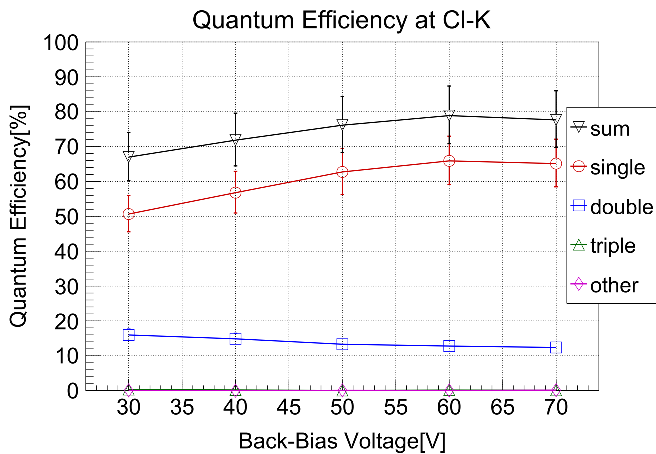

Fig. 9. Quantum efficiency of each grade with XRPIX2b-CZ-PZ at the energy of Cl-K X-rays as a function of V_{bb}.

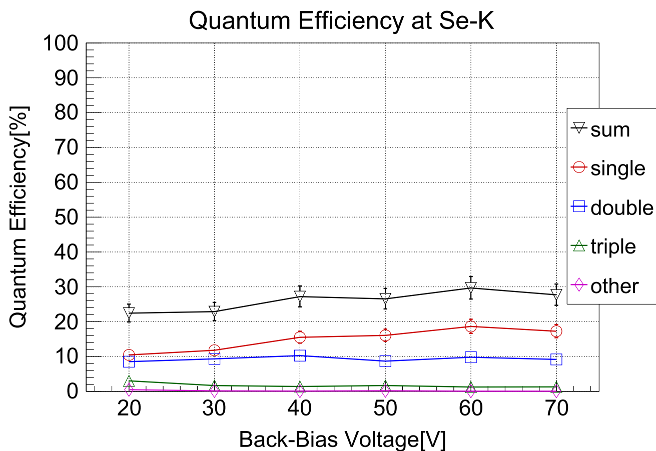

Fig. 10. Same as Fig. 9 but at the energy of Se-K X-rays.

layer will be 0.9–1.0 μm. It is significantly thinner than that of XRPIX2b-FZ-LA and can satisfy the requirement of 1.0 μm.

The thickness of the dead-layer measured with X-rays was larger than that of the phosphorus layer obtained with the SIMS and SRA. A similar result has been reported with a Pizza-processed SOIPIX sensor by [24]. Bautz et al. (2004) reported in the XIS BI device, MIT Lincoln Laboratory model CCID41, that the thickness of the dead layer based on the QE measurements is larger than the physical thickness of the SiO_2 and HfO_2 layer which was added by the chemisorption charging treatment [25]. Thus, it may be common among the back-side illuminated types of X-ray imagers that the measured thicknesses of dead layers with X-rays are larger than the physical thickness of the layers produced with semiconductor processes although the cause is unclear.

5. Summary and future

We have been developing fully depleted back-side illuminated types of XRPIXs, which have the sensitivity in 0.5–40 keV. We investigated the X-ray performance (2.6–12 keV) of the first two of them, namely XRPIX2b-FZ-LA and XRPIX2b-CZ-PZ, using our X-ray calibration system. XRPIX2b-FZ-LA is confirmed to have full depletion with a thickness of 500 μm, whereas the thickness of the back-side dead-layer is estimated to be 1.1–1.5 μm which is larger than the requirement of 1.0 μm. On the other hand, XRPIX2b-CZ-PZ, equipped with a thinner dead-layer, shows a higher QE in the soft X-ray band with the dead-layer thickness of 0.9–1.0 μm, even including an Al optical blocking layer of 0.2 μm. In order to improve the QE further in the soft X-ray energy band, we plan to test a BI-type of XRPIX3b with a low readout noise. We are also developing a new BI-type of XRPIXs, using a low-temperature chemical vapor deposition process on the back-side.

Acknowledgments

We acknowledge the valuable advice and great work by the personnel of LAPIS Semiconductor Co., Ltd. This study was supported by the Japan Society for the Promotion of Science (JSPS) KAKENHI Grant-in-Aid for Scientific Research on Innovative Areas 25109002 (Y.A.), 25109003 (S.K.) and 25109004 (T.G.T. & T.T.), Grant-in-Aid for Scientific Research (B) 23340047 (T.G.T.), Challenging Exploratory Research 26610047 (T.G.T.), Grant-in-Aid for Young Scientists (B) 15K17648 (A.T.) and Grant-in-Aid for JSPS Fellows 15J01842 (H.M.). This study was also supported by the VLSI Design and Education Center (VDEC), the University of Tokyo in collaboration with Cadence Design Systems, Inc., and Mentor Graphics, Inc.

References

[1] G.P. Garmire, et al., Advanced CCD imaging spectrometer (ACIS) instrument on the Chandra X-Ray Observatory, SPIE 4851 (2003) 28.
[2] M.J.L. Turner, et al., The European photon imaging camera on XMM-Newton: The MOS cameras, Astron. Astrophys. 365 (2001) L27.
[3] K. Koyama et al., X-Ray Imaging Spectrometers (XIS) on Board Suzaku.
[4] L. Strüder, et al., The European Photon Imaging Camera on XMM-Newton: The pn-CCD camera, Astron. Astrophysics. 365 (2001) L18. Publ. Astron. Soc. Jpn. 59 (2007) S22.
[5] T. Anada, T. Dotani, M. Ozaki, H. Murakami, Instrumental background of the X-ray CCD camera in space: Its dependence on the configuration parameters of CCD, Proc. SPIE 7011 (2008) 70113X.
[6] T. Takahashi, et al., Hard X-Ray Detector (HXD) on Board Suzaku, Publ. Astron. Soc. Jpn. 59 (2007) S35.
[7] M. Kokubun, et al., The hard X-ray Imager (HXI) for the ASTRO-H mission, Proc. SPIE 8443 (2012) 844325.
[8] T. Tsunemi, et al., Soft X-ray imager onboard ASTRO-H, Proc. SPIE 8859 (2013) 88590C.
[9] N. Meidinger, et al., Report on the eROSITA camera system, SPIE 9144 (2014) 91441W.
[10] N. Meidinger, et al., Development of the wide field imager for Athena, SPIE 9601 (2015) 96010H.
[11] A. Kenter, Monolithic CMOS imaging X-ray spectrometers, Proc. SPIE 9154 (2014) 91540J.
[12] G. Prigozhin, Measurement results for an X-ray 3D-integrated active pixel sensor, Proc. SPIE 7742 (2010) 77421I.

[13] C.V. Griffith, Recent progress and development of a Speedster-EXD—a new event-triggered hybrid CMOS X-ray detector, Proc. SPIE 9601 (2015) 96010B.
[14] T.G. Tsuru, et al., Development and performance of Kyoto's X-ray astronomical SOI pixel (SOIPIX) sensor, Proc. SPIE 9144 (2014) 914412.
[15] Y. Arai, et al., Development of SOI pixel process technology, Nucl. Instrum. Methods Phys. Res. A 636 (2011) S31.
[16] K. Hamaguchi, et al., X-ray CCD calibration system using fluorescent lines, Nucl. Instrum. Methods Phys. Res. A 450 (2012) 360.
[17] T. Uchida, Hardware-based TCP processor for gigabit Ethernet, IEEE Trans. Nucl. Sci. NS-55 (3) (2008) 1631.
[18] The quantum efficiency of the Silicon Drift Detector (Amptek XR-100) 〈http://www.amptek.com/products/xr-100sdd-silicon-drift-detector/〉.
[19] A.Takeda et al., Development and evaluation of an event-driven SOI pixel detector for X-ray astronomy, Proc. Sci. TIPP2014 (2014) 138.
[20] A. Takeda, et al., Improvement of spectroscopic performance using a charge-sensitive amplifier circuit for an X-ray astronomical SOI pixel detector, J. Instrum. 10 (2015) C06005.
[21] H. Matsumura, et al., Improving charge-collection efficiency of SOI pixel sensors for X-ray astronomy, Nucl. Instrum. Methods Phys. Res. A 794 (2015) 255.
[22] Ryu et al., First performance evaluation of an X-ray SOI pixel sensor for imaging spectroscopy and intra-pixel trigger, IEEE Trans. Nucl. Sci. NS-58 (5) (2011) 2528.
[23] Nakashima, et al., Progress in development of monolithic active pixel detector for X-ray astronomy with SOI CMOS technology, Phys. Procedia 37 (2012) 1373.
[24] M. Battaglia, et al., Characterisation of a thin fully depleted SOI pixel sensor with soft X-ray radiation, Nucl. Instrum. Methods Phys. Res. A 674 (2012) 51.
[25] M.W. Bautz, et al., Progress in X-ray CCD sensor performance for the Astro-E2 X-ray imaging spectrometer, SPIE 5501 (2004) 111.